SU(2)-Symmetric Spin-Boson Model: Quantum Criticality, Fixed-Point Annihilation, and Duality

Manuel Weber[1,2] and Matthias Vojta[2]
[1]*Max-Planck-Institut für Physik komplexer Systeme, Nöthnitzer Str. 38, 01187 Dresden, Germany*
[2]*Institut für Theoretische Physik and Würzburg-Dresden Cluster of Excellence ct.qmat, Technische Universität Dresden, 01062 Dresden, Germany*

(Received 17 March 2022; revised 5 August 2022; accepted 4 April 2023; published 1 May 2023)

The annihilation of two intermediate-coupling renormalization-group (RG) fixed points is of interest in diverse fields from statistical mechanics to high-energy physics, but has so far only been studied using perturbative techniques. Here we present high-accuracy quantum Monte Carlo results for the SU(2)-symmetric $S = 1/2$ spin-boson (or Bose-Kondo) model. We study the model with a power-law bath spectrum $\propto \omega^s$ where, in addition to a critical phase predicted by perturbative RG, a stable strong-coupling phase is present. Using a detailed scaling analysis, we provide direct numerical evidence for the collision and annihilation of two RG fixed points at $s^* = 0.6540(2)$, causing the critical phase to disappear for $s < s^*$. In particular, we uncover a surprising duality between the two fixed points, corresponding to a reflection symmetry of the RG beta function, which we utilize to make analytical predictions at strong coupling which are in excellent agreement with numerics. Our work makes phenomena of fixed-point annihilation accessible to large-scale simulations, and we comment on the consequences for impurity moments in critical magnets.

DOI: 10.1103/PhysRevLett.130.186701

A comprehensive understanding of critical phenomena requires one to unravel their underlying renormalization-group (RG) structure. A scenario of current interest is the collision and annihilation of two intermediate-coupling fixed points as a function of an external parameter, such as spatial dimension, as it leads to the breakdown of naive perturbative predictions and to an unconventionally slow RG flow close to the collision, associated with nontrivial crossover phenomena [1]. Fixed-point collisions have been discussed in a number of contexts using RG techniques, including the Abelian Higgs model [2,3], the chiral phase transition in quantum chromodynamics [1,4], the Q-state Potts model [5], and deconfined criticality in quantum magnets [6–8]. Detailed numerical studies are lacking, however, partly because dimensionality cannot be tuned continuously.

Dissipative quantum impurity models play a central role in modern physics, with applications from fundamental statistical mechanics to biological systems [9]. In condensed matter, they can serve as effective models for magnetic moments in magnets [10,11], but also for heavy-fermion metals described by extended dynamical mean-field theory (EDMFT) [12,13] as well as non-Fermi-liquid behavior in Sachdev-Ye-Kitaev-type (SYK-type) models [14,15]. Already simple dissipative impurity models can show nontrivial quantum phase transitions [9,16], and they have recently been proposed as platform to access fixed-point annihilation numerically [17,18], but direct evidence is missing.

It is the purpose of this Letter to close this gap. We utilize a recently developed wormhole quantum Monte Carlo (QMC) technique that enables us to simulate dissipative quantum systems to far lower temperatures than previously possible [19]. We study an SU(2)-symmetric three-bath generalization of the $S = 1/2$ spin-boson model [10,11,20,21], with a gapless bath spectrum scaling as ω^s. For this model, we firmly establish the existence of both critical and strong-coupling phases and obtain precise values for the critical exponents at the associated transition. The critical phase disappears from the phase diagram for $s < s^* = 0.6540(2)$ due to a collision of RG fixed points. Using a scaling analysis, we directly monitor this fixed-point collision in an unprecedented manner. Most importantly, we find a remarkable duality between the stable and unstable fixed points located at small and large intermediate coupling, respectively. This enables us to draw conclusions on the nature of the strong-coupling expansion and to deduce exact results near s^* even in the absence of a small parameter. Our work paves the way to high-accuracy studies of more complex dissipative quantum models and, for the first time, makes the fixed-point annihilation accessible to large-scale simulations.

Model and phase diagram.—The standard spin-boson model, where a spin-1/2 is subjected to a transverse field and coupled to a single bosonic bath, features a quantum phase transition between a delocalized and a localized phase [22,23]. This transition obeys a quantum-to-classical correspondence (QCC) [17,24,25], i.e., is in the same universality class as the thermal phase transition of the one-dimensional Ising model with $1/r^{1+s}$ interactions [26]. Generalizations of the model to multiple baths have been found to show more complex behavior. In particular, the existence of a nonclassical critical phase has been predicted using perturbative RG and large-N techniques [10,11,20,21]. For the two-bath case, extensive numerical results have been obtained using matrix-product-state (MPS) techniques [17,18]; they confirmed the absence of QCC, but also signaled that the perturbative prediction becomes invalid for small s where only a strong-coupling phase was shown to exist. For the more relevant SU(2)-symmetric three-bath case, high-accuracy results are lacking, as established numerical methods such as MPS [17] and Wilson's numerical renormalization group [23,27] become prohibitively expensive. Consequently, relatively little precise information is available on the phases and transitions of this model [28,29]. This is pressing since a number of conclusions drawn in earlier work rely on extrapolating the perturbative ϵ-expansion results to $\epsilon = 1 - s \to 1$ [10–13].

In this Letter, we consider this three-bath generalization of the spin-boson model,

$$\mathcal{H} = \sum_{i=x,y,z} \sum_{q} [\lambda_{qi} S^i (\hat{B}_{qi} + \hat{B}_{qi}^\dagger) + \omega_q \hat{B}_{qi}^\dagger \hat{B}_{qi}]. \quad (1)$$

Here, an $S = 1/2$ spin $\vec{S}$ is coupled to three independent bosonic baths, whose spectral densities $J_i(\omega) = \pi \sum_q \lambda_{qi}^2 \delta(\omega - \omega_q)$ are of power-law form,

$$J_i(\omega) = 2\pi \alpha_i \omega_c^{1-s} \omega^s, \qquad 0 < \omega < \omega_c = 1, \quad (2)$$

with ω_c being a cutoff energy. The model (1) displays nontrivial quantum dynamics even in the absence of an additional external field: The noncommuting character of the three spin components implies that the localization tendencies induced by each bath compete. The α_i measure the dissipation strength, and we focus on the SU(2)-symmetric case $\alpha_i \equiv \alpha$.

Figure 1(a) displays the model's quantitative phase diagram obtained from our QMC simulations. For bath exponents $s^* < s < 1$, both critical (CR) and localized (L) phases exist and are separated by a continuous quantum phase transition. In contrast, for $s > 1$ the model is always in a free-spin (F) phase, whereas for $s < s^*$ any finite coupling drives the system into the L phase. This L phase

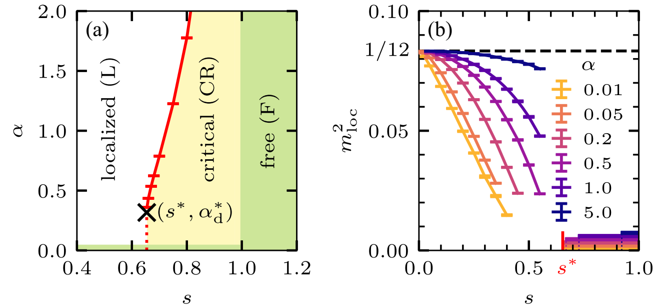

FIG. 1. (a) Phase diagram as a function of the bath exponent s and the spin-boson coupling α. The line of second-order quantum phase transitions (red) between the CR and L phases terminates at the point (s^*, α_d^*), such that the CR phase disappears for $s < s^*$; for details see text. (b) Local moment $m_{\rm loc}^2 = \lim_{\beta\to\infty} \langle S^x(\beta/2) S^x(0) \rangle$ for different α. We only show data that are converged in temperature. For each α, the corresponding horizontal line in the lower right corner marks the onset of the CR phase where $m_{\rm loc}^2 = 0$ for $s > s(\alpha_{\rm QC})$. The dashed line corresponds to $m_{\rm loc}^2(\alpha \to \infty) = S^2/3 = 1/12$.

exhibits spontaneous breaking of the SU(2) symmetry, whereas the F phase features an asymptotically free spin. Finally, the CR phase is characterized by fractional power-law spin correlations [10,11,14], $\chi_i(\omega) \propto \omega^{-x}$ where $\chi_i(\tau) = \langle S^i(\tau) S^i(0) \rangle \sim 1/\tau^{1-x}$.

Perturbative RG and fixed-point collision.—Before we discuss the details of our numerical results, we review what is known about the fixed-point structure from weak-coupling perturbative RG [11,30]. The impurity–bath coupling is marginal at $s = 1$, and expanding about the $\alpha = 0$ free-spin fixed point results in the two-loop beta function [30,31],

$$\beta(\alpha) \equiv \frac{d\alpha}{d \ln \mu} = -(1-s)\alpha + 4\alpha^2 - 8\alpha^3, \quad (3)$$

where μ is the RG reference scale. From this beta function, one deduces the existence of an infrared-stable fixed point for $s < 1$, located at

$$\alpha_{\rm CR}^* = \frac{1-s}{4} + \frac{(1-s)^2}{8} + \mathcal{O}[(1-s)^3]; \quad (4)$$

this is the CR fixed point corresponding to the CR phase. Its properties can be obtained in a double expansion in α and $(1 - s)$. The power-law spin autocorrelations are characterized by the exponent x, and $x = s$ is an exact result following from the diagrammatic structure of the susceptibility [11,30].

The two-loop beta function in Eq. (3) does display *two* nontrivial fixed points at $\alpha_{1,2}^* = \frac{1}{4}[1 \pm \sqrt{1 - 2(1-s)}]$, with α_2^* being the stable CR fixed point of Eq. (4), and α_1^* being infrared unstable. These two fixed points approach each other upon decreasing s from unity, such that they

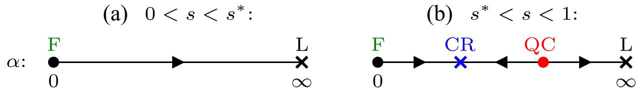

FIG. 2. Schematic RG flow for (a) $0 < s < s^*$ and (b) $s^* < s < 1$.

collide as $s \to s^{*,+}$, with $s^* = 1/2$ from (3). Although α_1^* is outside the regime of validity of the epsilon expansion, the comparison with numerics suggests to identify α_1^* with the quantum critical (QC) fixed point controlling the transition between the CR and L phases.

The resulting schematic RG flow is depicted in Fig. 2: Two intermediate-coupling fixed points exist for $s^* < s < 1$, while they disappear for $s < s^*$ leaving only runaway flow to strong coupling. As we show below, our numerical results not only prove this picture to be correct but also indicate a surprising duality between the CR and QC fixed points; below, we will use this duality with Eqs. (3) and (4) to make analytical predictions at strong coupling.

QMC method.—For our simulations, we used an exact QMC method with global wormhole updates [19] that samples a diagrammatic expansion of the partition function in the retarded spin interaction [32], originating from tracing out the bosonic bath in Eq. (1) analytically. A detailed description of our method can be found in Ref. [19].

QMC results.—To determine the phase diagram in Fig. 1(a), we calculate the dynamical spin susceptibility $\chi_x(\mathrm{i}\Omega_n) = \int_0^\beta d\tau\, e^{\mathrm{i}\Omega_n\tau}\langle S^x(\tau)S^x(0)\rangle$ from the imaginary-time spin correlations in the x direction. Here, $\Omega_n = 2\pi n/\beta$, $n \in \mathbb{Z}$, are the bosonic Matsubara frequencies and $\beta = 1/T$ is the inverse temperature. The different phases in Fig. 1(a) can be identified from the low-temperature behavior of the static susceptibility $\chi_x \equiv \chi_x(\mathrm{i}\Omega_0)$: At $\alpha = 0$, $\chi_x(T) = 1/(4T)$. In the F and L phases, $\chi_x(T) = m_{\mathrm{loc}}^2/T$ follows a Curie law as $T \to 0$ with a reduced but finite local moment; the latter is determined as $m_{\mathrm{loc}}^2 = \lim_{\beta\to\infty}\langle S^x(\beta/2)S^x(0)\rangle$ and shown in Fig. 1(b). We find that $m_{\mathrm{loc}}^2(s \to 0)$ approaches the strong-coupling result $m_{\mathrm{loc}}^2(\alpha \to \infty) = S^2/3 = 1/12$ of the L phase independent of α; this is the local moment of a classical spin. In the CR phase, $m_{\mathrm{loc}}^2 = 0$ and $\chi_x(T) \propto T^{-s}$. For further details, see the Supplemental Material [33].

For a quantitative analysis of criticality, we consider the correlation length along the imaginary-time axis (correlation time), $\xi_x = (1/\Omega_1)\sqrt{\chi_x(\mathrm{i}\Omega_0)/\chi_x(\mathrm{i}\Omega_1) - 1}$. In analogy to the definition of the spatial correlation length [33,37], we identify the inverse temperature β with the system size in the imaginary-time direction and the Matsubara frequency Ω_0 with the ordering vector [note that the lowest Matsubara frequencies determine the long-time decay of $\chi_x(\tau)$]. Figure 3(a) depicts ξ_x/β as a function of α for $s = 0.75$ and different temperatures. We find that ξ_x/β diverges in the L phase, but remains finite in the CR phase. Because ξ_x/β becomes an RG-invariant quantity at the fixed points of the beta function, we can identify the two sharp crossings observed in the insets of Fig. 3(a) with the corresponding fixed-point couplings α_{CR} and α_{QC}. Moreover, Fig. 3(b) demonstrates that ξ_x/β fulfills the scaling ansatz

$$\xi_x/\beta = f(\beta^{1/\nu}(\alpha - \alpha_{\mathrm{QC}})) \tag{5}$$

near the critical coupling α_{QC}. Here, ν is the correlation-length exponent and f is a universal function. We observe a clear data collapse over many orders of magnitude in the energy scale $T/|\alpha - \alpha_{\mathrm{QC}}|^\nu$ and for temperatures $T/\omega_c \lesssim 10^{-3}$. Details on how we estimate α_{CR}, α_{QC}, and ν are provided in the Supplemental Material [33].

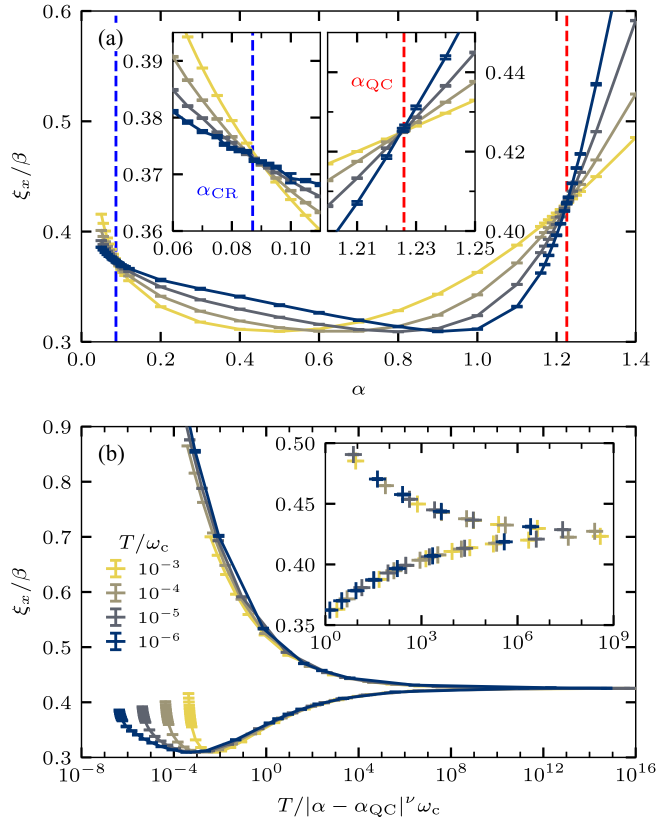

FIG. 3. (a) Correlation length ξ_x/β as a function of α for different temperatures and $s = 0.75$. The insets show close-ups of the crossings near the CR and QC fixed points. (b) Data collapse for ξ_x/β near the QC fixed point. The inset shows a detailed view of the critical region. Finite-size scaling yields $1/\nu = 0.192(2)$ [33].

Figure 4 shows the critical exponents as a function of s. The correlation-length exponent ν estimated from Eq. (5) diverges for both $s \to 1$ and $s \to s^*$ [see Fig. 4(a)] and the leading behavior is consistent with the predictions (8) and (9) derived below. As demonstrated in the Supplemental Material [33], the remaining exponents are completely

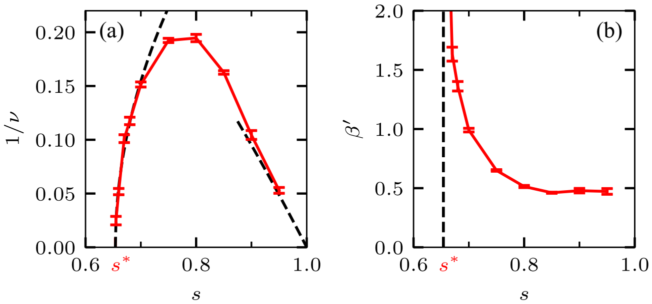

FIG. 4. (a) Inverse correlation-length exponent $1/\nu$ associated with the QC fixed point as a function of s. ν diverges for both $s \to 1$ and $s \to s^*$. The dashed lines show the predictions (8) and (9) based on fixed-point duality; for the latter, we fit $\sqrt{A_1 B_0} = 0.72(2)$. (b) Magnetization exponent β' calculated from $1/\nu$ via the hyperscaling relation $\beta'/\nu = (1-s)/2$.

determined by hyperscaling relations. Close to criticality, the local moment fulfills $m_{\mathrm{loc}} \propto (\alpha - \alpha_{\mathrm{QC}})^{\beta'}$. The magnetization exponent β' is summarized in Fig. 4(b); it approaches $\beta' \approx 1/2$ for $s \to 1$, but diverges for $s \to s^*$. This divergence results from the fixed-point collision and leads to an extremely slow RG flow for intermediate α and $s \sim s^*$ [1]. In particular, the order parameter m_{loc} is exponentially suppressed [33] in the region $\alpha < \alpha_{\mathrm{d}}^*$ and $s \lesssim s^*$ in Fig. 1(b), such that a naive extrapolation of m_{loc}^2 to zero would significantly underestimate s^*. This is likely the reason why the value of s^* as estimated in Ref. [29] significantly deviates from ours. We also note that such a fixed-point collision is not present in any of the relevant classical spin models, hence QCC is violated for the model under consideration.

Figure 5(a) shows the evolution of α_{CR} and α_{QC} as a function of $(1-s)$. For small $(1-s)$, the former closely follows the RG prediction (4), whereas the latter diverges proportional to $1/(1-s)$. Remarkably, the evolution of α_{CR} and α_{QC} as a function of $(1-s)$ is almost symmetric in $\ln(\alpha)$ until they coalesce at $(s^*, \alpha_{\mathrm{d}}^*)$. The fixed-point collision appears at $s^* = 0.6540(2)$ and $\alpha_{\mathrm{d}}^* = 0.317(1)$, which we estimate from a quadratic fit in $\ln(\alpha)$, as shown in Fig. 5(b). As a function of s, the product $\alpha_{\mathrm{CR}} \times \alpha_{\mathrm{QC}}$ in Fig. 5(c) varies by around 10%, which is approximately constant considering that each coupling varies over several orders of magnitude.

Duality.—The data in Fig. 5 show that the two zeros of the (exact) beta function are located symmetrically with respect to $\ln(\alpha_{\mathrm{d}}^*)$ for all s to very good accuracy, hence $\alpha_{\mathrm{QC}}/\alpha_{\mathrm{d}}^* = \alpha_{\mathrm{d}}^*/\alpha_{\mathrm{CR}}$. We conjecture that this symmetry is obeyed by the full beta function, $(1/\alpha)\beta(\alpha) = \tilde{\beta}(\alpha/\alpha_{\mathrm{d}}^*)$ with $\tilde{\beta}(x) = \tilde{\beta}(1/x)$, see Fig. 6. This implies a duality between the two fixed-point theories which we discuss in the following.

First, the properties of QC near $s = 1$ can be deduced from the dual of the weak-coupling expansion (3); we note

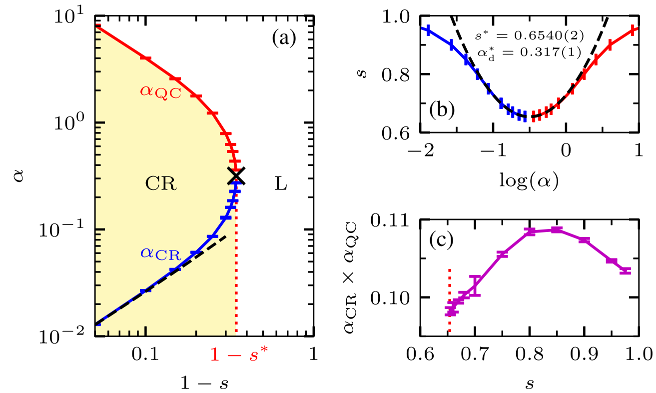

FIG. 5. Fixed-point duality. (a) Location of the two intermediate-coupling fixed points CR and QC, as determined from crossing points of $T^s\chi_x$ [33], as a function of the bath exponent s. The black dashed line indicates the prediction (4) of the perturbative RG for α_{CR}. (b) Close to s^*, the fixed-point collision is well approximated by $s = s^* + (B_0/A_1)\ln^2(\alpha/\alpha_{\mathrm{d}}^*)$ from which we extract $s^* = 0.6540(2)$, $\alpha_{\mathrm{d}}^* = 0.317(1)$ where the fixed points disappear, and $A_1/B_0 = 17.7(2)$. (c) Product of the two fixed-point couplings as a function of s: This is approximately constant despite the couplings varying over several orders of magnitude.

that a suitable field theory for that is not known. Introducing $\bar{\alpha} \equiv \alpha_{\mathrm{d}}^{*2}/\alpha$, we have by duality

$$\beta(\bar{\alpha}) = (1-s)\bar{\alpha} - 4\bar{\alpha}^2 + 8\bar{\alpha}^3, \tag{6}$$

where the sign change compared to (3) arises from $d\ln\alpha/d\ln\mu = -d\ln(1/\alpha)/d\ln\mu$. The QC fixed point is then located at

$$\bar{\alpha}_{\mathrm{QC}}^* = \frac{1-s}{4} + \frac{(1-s)^2}{8} + \mathcal{O}[(1-s)^3], \tag{7}$$

and its correlation-length exponent is obtained from expanding $\beta(\bar{\alpha})$ about $\bar{\alpha}_{\mathrm{QC}}^*$, resulting in

$$1/\nu = 1 - s - \frac{(1-s)^2}{2} + \mathcal{O}[(1-s)^3]. \tag{8}$$

Second, to study the fixed-point annihilation at s^*, we expand the beta function near α_{d}^* as $\beta(\alpha) = A(s) - B(s)\ln^2(\alpha/\alpha_{\mathrm{d}}^*)$ [1], with $A(s) = A_1(s - s^*)$ and $B(s) = B_0(s^*) + B_1(s - s^*)$. This yields the locations of the two

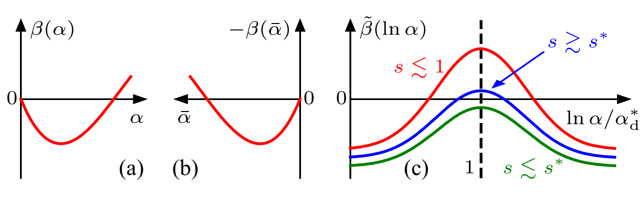

FIG. 6. (a) Weak-coupling and (b) its dual strong-coupling beta function, as in Eqs. (3) and (6). (c) Reflection symmetry of $\tilde{\beta}(\ln\,\alpha)$ around α_{d}^*. The zeros of $\beta(\alpha)$ disappear for $s < s^*$.

fixed points as $\pm\ln(\alpha^*/\alpha_{\rm d}^*) = \sqrt{A_1/B_0}\sqrt{s-s^*}$ and the correlation-length exponent of QC as

$$1/\nu = \sqrt{A_1 B_0}\sqrt{s-s^*}. \tag{9}$$

Both predictions (8) and (9) are in good agreement with the QMC data in Fig. 4.

While Eq. (9) generically applies near a fixed-point collision, Eqs. (7) and (8) rely on the conjectured mirror symmetry of the beta function. Our numerics indicate that this symmetry is not exact, hence the weak- and strong-coupling expansions possibly differ in higher loop orders.

Impurities in quantum critical magnets.—Previous work [10,11] on magnetic impurities in quantum critical magnets in $d = 3 - \epsilon$ space dimensions—a problem closely related to the three-bath spin-boson model—employed a weak-coupling expansion similar to that in Eq. (3), with the difference that interactions among the bath bosons are RG relevant for $d < 3$. The physically most interesting case of $d = 2$ corresponds to a bath exponent of $s = 0$. References [10,11] assumed continuity from small $\epsilon = 1 - s$ to $\epsilon = 1$, and numerical results have been interpreted in terms of the CR fixed point [38]. Given that this continuity does *not* hold for the noninteracting bath case studied here, the present results raise the interesting question whether a strong-coupling phase also occurs for the impurity-in-a-magnet problem and, if yes, what its properties are.

Relatedly, conclusions which were drawn from ϵ or large-N expansion results for quantum critical lattice models in the framework of EDMFT [12,13,29] need to be revisited.

Conclusions.—Using high-accuracy QMC simulations, we have determined the phase diagram and critical properties of the SU(2)-symmetric spin-boson model. For the first time, we were able to extract the location of both intermediate-coupling fixed points using a scaling analysis and to monitor their collision and subsequent annihilation as a function of the bath exponent s. The fixed points display a remarkable duality, which we have utilized to deduce analytical results at strong coupling; we hope that future studies will give further insight into this novel duality relation. Our results illustrate the power of the QMC algorithm of Ref. [19], which makes the analysis of unconventionally slow RG flow near the collision [1] accessible to future numerical studies. In the context of SYK models, it has been suggested that the localized phase of the single-impurity problem triggers the existence of an SYK spin-glass state [15]; the role of the fixed-point annihilation is an interesting open problem.

We thank F. Parisen Toldin for helpful discussions. This work has been supported by the Deutsche Forschungsgemeinschaft through the Würzburg-Dresden Cluster of Excellence on Complexity and Topology in Quantum Matter—*ct.qmat* (EXC 2147, Project No. 390858490) and SFB 1143 on Correlated Magnetism (Project No. 247310070).

Note added.—Recently, we became aware of Refs. [39–41] in which the fixed-point annihilation is studied analytically in the large-S limit. These results indicate that the duality relation of the beta function becomes exact for $S \to \infty$, but this is not discussed in Refs. [39–41].

[1] D. B. Kaplan, J.-W. Lee, D. T. Son, and M. A. Stephanov, Phys. Rev. D **80**, 125005 (2009).
[2] B. I. Halperin, T. C. Lubensky, and S.-k. Ma, Phys. Rev. Lett. **32**, 292 (1974).
[3] J. Braun, H. Gies, L. Janssen, and D. Roscher, Phys. Rev. D **90**, 036002 (2014).
[4] H. Gies and J. Jaeckel, Eur. Phys. J. C **46**, 433 (2006).
[5] B. Nienhuis, A. N. Berker, E. K. Riedel, and M. Schick, Phys. Rev. Lett. **43**, 737 (1979).
[6] A. Nahum, J. T. Chalker, P. Serna, M. Ortuño, and A. M. Somoza, Phys. Rev. X **5**, 041048 (2015).
[7] C. Wang, A. Nahum, M. A. Metlitski, C. Xu, and T. Senthil, Phys. Rev. X **7**, 031051 (2017).
[8] A. Nahum, Phys. Rev. B **102**, 201116(R) (2020).
[9] A. J. Leggett, S. Chakravarty, A. T. Dorsey, M. P. A. Fisher, A. Garg, and W. Zwerger, Rev. Mod. Phys. **59**, 1 (1987).
[10] S. Sachdev, C. Buragohain, and M. Vojta, Science **286**, 2479 (1999).
[11] M. Vojta, C. Buragohain, and S. Sachdev, Phys. Rev. B **61**, 15152 (2000).
[12] Q. Si, S. Rabello, K. Ingersent, and J. L. Smith, Nature (London) **413**, 804 (2001).
[13] Q. Si, S. Rabello, K. Ingersent, and J. L. Smith, Phys. Rev. B **68**, 115103 (2003).
[14] S. Sachdev and J. Ye, Phys. Rev. Lett. **70**, 3339 (1993).
[15] D. Chowdhury, A Georges, O. Parcollet, and S. Sachdev, Rev. Mod. Phys. **94**, 035004 (2022).
[16] M. Vojta, Philos. Mag. **86**, 1807 (2006).
[17] C. Guo, A. Weichselbaum, J. von Delft, and M. Vojta, Phys. Rev. Lett. **108**, 160401 (2012).
[18] B. Bruognolo, A. Weichselbaum, C. Guo, J. von Delft, I. Schneider, and M. Vojta, Phys. Rev. B **90**, 245130 (2014).
[19] M. Weber, Phys. Rev. B **105**, 165129 (2022).
[20] J. L. Smith and Q. Si, Europhys. Lett. **45**, 228 (1999).
[21] A. M. Sengupta, Phys. Rev. B **61**, 4041 (2000).
[22] S. K. Kehrein and A. Mielke, Phys. Lett. A **219**, 313 (1996).
[23] R. Bulla, N. H. Tong, and M. Vojta, Phys. Rev. Lett. **91**, 170601 (2003).
[24] M. Vojta, N. H. Tong, and R. Bulla, Phys. Rev. Lett. **94**, 070604 (2005); **102**, 249904(E) (2009).
[25] A. Winter, H. Rieger, M. Vojta, and R. Bulla, Phys. Rev. Lett. **102**, 030601 (2009).
[26] M. E. Fisher, S. K. Ma, and B. G. Nickel, Phys. Rev. Lett. **29**, 917 (1972).
[27] R. Bulla, H. J. Lee, N. H. Tong, and M. Vojta, Phys. Rev. B **71**, 045122 (2005).
[28] J. Otsuki, Phys. Rev. B **87**, 125102 (2013).

[29] A. Cai and Q. Si, Phys. Rev. B **100**, 014439 (2019).
[30] L. Zhu and Q. Si, Phys. Rev. B **66**, 024426 (2002); G. Zarand and E. Demler, Phys. Rev. B **66**, 024427 (2002).
[31] α and $\bar{\alpha}$ in Eqs. (3), (4), (6), and (7) represent renormalized couplings in the RG framework (as opposed to bare couplings; for notational simplicity, we use the same symbol for both). Their definition depends on the RG scheme; our choice differs by a factor of 2 from that of Ref. [30] to match α_{CR} to the microscopic calculation.
[32] M. Weber, F. F. Assaad, and M. Hohenadler, Phys. Rev. Lett. **119**, 097401 (2017).
[33] See Supplemental Material at http://link.aps.org/supplemental/10.1103/PhysRevLett.130.186701 for additional results for the local-moment formation, details on our finite-size scaling analysis, and a numerical confirmation of hyperscaling, which includes Refs. [34–36].
[34] M. Campostrini, A. Pelissetto, and E. Vicari, Phys. Rev. B **89**, 094516 (2014).
[35] F. Parisen Toldin, M. Hohenadler, F. F. Assaad, and I. F. Herbut, Phys. Rev. B **91**, 165108 (2015).
[36] B. Bruognolo, Master's thesis, LMU Munich, 2013.
[37] A. W. Sandvik, AIP Conf. Proc. **1297**, 135 (2010).
[38] K. H. Hoglund and A. W. Sandvik, Phys. Rev. Lett. **99**, 027205 (2007).
[39] G. Cuomo, Z. Komargodski, M. Mezei, and A. Raviv-Moshe, J. High Energy Phys. 06 (2022) 112.
[40] M. Beccaria, S. Giombi, and A. Tseytlin, J. Phys. **55**, 255401 (2022).
[41] A. Nahum, Phys. Rev. B **106**, L081109 (2022).